

Optical investigation of $\text{BaFe}_2(\text{As}_{0.77}\text{P}_{0.23})_2$: Spin-fluctuation-mediated superconductivity under pressure

E. Uykur,^{1,*} T. Kobayashi,² W. Hirata,² S. Miyasaka,² S. Tajima,² and C. A. Kuntscher^{1,†}

¹*Experimentalphysik 2, Universität Augsburg, D-86159 Augsburg, Germany*

²*Department of Physics, Graduate School of Science, Osaka University, Osaka 560-0043, Japan*

(Received 13 March 2017; revised manuscript received 1 June 2017; published 22 June 2017)

Temperature-dependent reflectivity measurements in the frequency range 75–8000 cm^{-1} were performed on $\text{BaFe}_2(\text{As}_{0.77}\text{P}_{0.23})_2$ single crystals under pressure up to ~ 5 GPa. The obtained optical conductivity spectra have been analyzed to extract the electron-boson spectral density $\alpha^2 F(\Omega)$. A sharp resonance peak was observed in $\alpha^2 F(\Omega)$ upon the superconducting transition, persisting throughout the applied pressure range. The energy and temperature dependences of this peak are consistent with the superconducting gap opening. Furthermore, several similarities with other experimental probes such as inelastic neutron scattering (INS) [D. S. Inosov *et al.*, *Nat. Lett.* **6**, 178 (2010)] give evidence for the coupling to a bosonic mode, possibly due to spin fluctuations. Moreover, electronic correlations have been calculated via spectral weight analysis, which revealed that the system stays in the strongly correlated regime throughout the applied pressure range. However, a comparison to the parent compound showed that the electronic correlations are slightly decreased with P doping. The investigation of the phase diagram obtained by our optical study under pressure also revealed the coexistence of the spin-density wave and the superconducting regions, where the coexistence region shifts to the lower pressure range with increasing P content. Moreover, the optimum pressure range, where the highest superconducting transition temperature has been obtained, shows a nonlinear decrease with increasing P content.

DOI: [10.1103/PhysRevB.95.214512](https://doi.org/10.1103/PhysRevB.95.214512)

I. INTRODUCTION

The pressure-induced superconducting (SC) state in iron pnictide (Fe-Pn) high-temperature superconductors has been addressed by several transport and magnetic measurements [1–8]. It has been shown that the external pressure has similar effects like the chemical doping (electron, hole, or isotropic carrier doping) and gives a very similar phase diagram [9–11]. The suppression of the magnetically ordered [spin-density wave (SDW)] state below the magnetic transition temperature T_N and the emergence of the SC state for temperatures below the superconducting transition temperature T_c were found in both cases. Despite the intensive work done on these systems, however, there is no report regarding the nature of the SC state induced by external pressure. External pressure is a clean way to induce superconductivity and does not introduce any additional impurities to the system. Therefore, the investigation of the mechanism for the pressure-induced SC state may give valuable information of the intrinsic properties of Fe-Pn superconductors.

For the conventional BCS-type superconductors, superconductivity emerges due to electron-phonon interactions [12]. For unconventional superconductors such as high-temperature cuprates and iron pnictides, on the other hand, there is no consensus yet on the underlying pairing mechanism reached [13–18]; therefore, it is necessary to perform further studies to reveal this issue. In that sense, the inelastic charge carrier scattering is a valuable experimental technique for studying superconducting materials since it provides information about the underlying mechanism of the superconductivity.

The inelastic charge carrier scattering can be investigated with several experimental techniques such as angle-resolved photoemission spectroscopy (ARPES) [19], Raman scattering [20], scanning tunneling spectroscopy (STS) [21], and infrared spectroscopy [22]. As the primary technique of the current study, infrared spectroscopy has been widely used to obtain the electron-boson spectral density. One extracts the density of the bosonic excitations from experimental scattering data and compares it with other known data obtained from other techniques such as inelastic neutron scattering (INS), band calculations, etc. Studies on the conventional superconductors revealed that the obtained electron-boson spectral density is consistent with the phonons [23]. In contrast, studies on cuprates reported the electron-boson spectral density associated with other mechanisms, such as spin fluctuations, which was supported by other experiments and theoretical works as well [14,24–28]. Similar studies were also performed on Fe-Pn superconductors, where the SC state is induced by chemical substitution, where several similarities to the cuprates have been shown [29–33]. One should note, however, that Fe-Pn superconductors are multiband systems, unlike cuprates, and show different gap symmetry [16,17]. Moreover, such studies do not exist for the pressure-induced superconducting state of Fe-Pn superconductors.

In this study, we focus on the pressure-induced optical properties of the so-called 122 system, specifically on P-doped BaFe_2As_2 in the underdoped regime. A detailed analysis of the SDW and SC state for the BaFe_2As_2 parent compound has already been presented in our previous study [34]. In this study, we will mainly discuss our findings for the $\text{BaFe}_2(\text{As}_{0.77}\text{P}_{0.23})_2$ compound, and the results of the parent compound are given as a comparison and discussed in terms of electronic correlations, superconducting gap, and pressure effects.

*ece.uykur@physik.uni-augsburg.de

†christine.kuntscher@physik.uni-augsburg.de

II. EXPERIMENT

$\text{BaFe}_2(\text{As}_{0.77}\text{P}_{0.23})_2$ single crystals were grown using the self-flux method and annealed as described elsewhere [35,36]. They are superconducting at ambient pressure with a transition temperature $T_c = 14.2 \pm 1$ K. Samples were polished down to $0.1\text{-}\mu\text{m}$ surface roughness and cut into small pieces with a typical size of $\sim 250 \times 250 \times 60 \mu\text{m}^3$. They were placed into a type-IIa diamond-anvil cell (DAC) [37], and finely ground CsI powder was used as quasihydrostatic pressure-transmitting medium. The pressure in the DAC was measured *in situ* with the ruby luminescence method [38] for each temperature separately.

Temperature-dependent reflectivity measurements were performed from ~ 75 to 8000 cm^{-1} between 6 and 300 K. The measured pressure range extends up to ~ 5 GPa. A home-built measurement system described elsewhere [39] was used for the measurements. The reflectivity spectra were measured at the sample-diamond interface, using the CuBe gasket inside the DAC as reference. Above 8000 cm^{-1} the reflectivity spectrum shows no significant pressure or temperature dependence. Therefore, for further analysis, the ambient-condition (ambient pressure, room temperature) reflectivity spectrum of $\text{BaFe}_2(\text{As}_{0.77}\text{P}_{0.23})_2$ measured in an IR microscope coupled with an IFS 66 Fourier transform infrared (FTIR) spectrometer up to 20000 cm^{-1} and the reflectivity spectrum of the parent BaFe_2As_2 compound obtained at UVSOR, Institute for Molecular Science (Okazaki, JAPAN), up to 40 eV were used.

Between 1700 and 2800 cm^{-1} the multiphonon absorption of the diamond anvil affects the measured reflectivity spectra, and therefore, this energy range has been interpolated with the Drude-Lorentz fitting of the reflectivity spectra. The low-energy region has been extrapolated with the Drude-Lorentz fitting of the reflectivity spectra for further analysis. The optical conductivity spectra have been calculated by Kramers-Kronig (KK) transformation [40] of the measured reflectivity. The so-obtained optical conductivity spectra are in good agreement with the spectra based on a Drude-Lorentz fitting of the measured reflectivity data.

III. RESULTS AND DISCUSSION

A. Optical conductivity under pressure

The pressure evolution of the optical conductivity for $\text{BaFe}_2(\text{As}_{0.77}\text{P}_{0.23})_2$ is shown in Fig. 1. At 1.3 GPa (the lowest pressure measured in this study), the sample shows a metallic behavior at high temperatures [see Fig. 1(a)]. Below 60 K the magnetically ordered state is entered, and the spin-density-wave order is visible in the optical conductivity spectra: While the overall spectral weight (SW) is suppressed below $\sim 300 \text{ cm}^{-1}$, it is recovered as a small absorption peak at around 700 cm^{-1} . In the inset of Fig. 1(a), we plot the ratio of the SW [where $\text{SW} = \int_0^{\omega_{\text{cutoff}}} \sigma_1(\omega) d\omega$, with ω_{cutoff} being the measured energy range] at 60 and 20 K with respect to 100 K (which is just above the SDW transition). This ratio shows the energy scale of the SW transfer. In the case of a SW transfer from low energies to the high-energy range, the ratio will drop below 1 until the overall energy range of the SW transfer is observed. Accordingly, the overall SW is recovered at $\sim 1200 \text{ cm}^{-1}$. With further cooling down a small

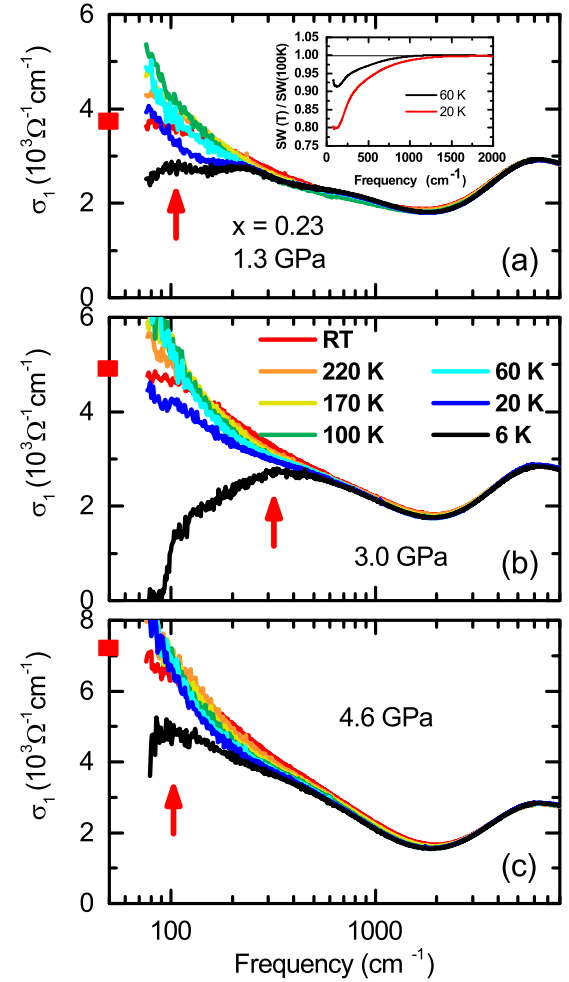


FIG. 1. Temperature-dependent optical conductivity of $\text{BaFe}_2(\text{As}_{0.77}\text{P}_{0.23})_2$ at (a) 1.3, (b) 3.0, and (c) 4.6 GPa. Solid squares at $\omega = 0$ are dc conductivity values obtained from the Hagen-Rubens fitting of the measured reflectivity spectra. Red arrows mark the suppression of the optical conductivity with SC gap opening. Inset: Spectral weight ratio below the SDW transition at 1.3 GPa. The SW transfer from low energies to high energies, and the recovery of the overall SW below $\sim 1200 \text{ cm}^{-1}$ is demonstrated.

downturn of the optical conductivity below $\sim 120 \text{ cm}^{-1}$ can be seen in the spectra (red arrow), with no spectral weight recovery being observed. This indicates the superconducting transition. A full transition has not been observed, probably due to an insufficient lower temperature (6 K is almost half of the transition) and/or a limited low-energy range.

With increasing pressure the SDW state is suppressed, while the SC transition temperature and the SC gap increase. At 3.0 GPa, the metallic behavior at higher temperatures changes to a slight suppression of the low-energy optical conductivity below 20 K, which becomes more pronounced with a further decrease in temperature [see Fig. 1(b)]. At the lowest measured temperature, 6 K, the optical conductivity is completely suppressed below 90 cm^{-1} , indicating superconductivity with a nodeless energy gap at around 3.0 GPa. A further increase in pressure suppresses the superconducting gap, and at 4.6 GPa

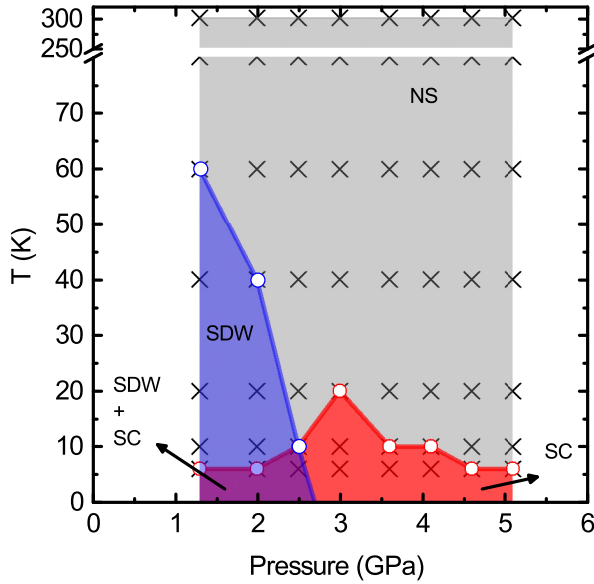


FIG. 2. Pressure-temperature phase diagram of BaFe₂(As_{0.77}P_{0.23})₂ obtained from the current optical study. Crosses are the measured P - T points. The normal state (gray shading), SDW state (blue shading), SC state (red shading), and coexistence region (purple shading) are depicted. The P - T values, where we start to observe SDW- and SC-state-related features, are given with open blue and red circles, respectively.

only a small downturn without a full suppression at lower energies is observed [see Fig. 1(c)].

The solid squares in Fig. 1 indicate the dc conductivity values obtained from the Hagen-Rubens fitting of the measured reflectivity spectra for each pressure at room temperature. The smooth extrapolation of the room-temperature optical conductivity to the obtained dc values confirms the reliability of our KK transformation. With increasing pressure the dc conductivity is increasing, indicating the increase of the metallicity of the system with pressure, which is consistent with the reported electrical transport measurements [5,9]. Furthermore, the energy dependence of the SC gap feature of the optical conductivity (shown with red arrows in Fig. 1) first increases with pressure, gives a maximum at 3 GPa, and decreases with a further increase of the pressure. The various phases of BaFe₂(As_{0.77}P_{0.23})₂ as a function of pressure and temperature are summarized in the P - T phase diagram shown in Fig. 2. Here, T_N and T_c have been determined from the optical conductivity as the temperatures where we start to observe the SDW- and SC-related signatures, respectively.

B. Optical scattering rate under pressure

The optical scattering rate can be obtained through extended Drude analysis of the complex optical conductivity by using the generalized Drude formula [41]:

$$\sigma(T, \omega) = \frac{\Omega_p^2}{4\pi} \frac{1}{1/\tau(\omega) - i\omega[1 + \lambda(\omega)]}. \quad (1)$$

Here, $\Omega_p^2 = 4\pi n e^2 / m$ is the square of the plasma frequency, where n is the carrier density and m is the effective mass.

Then, the optical scattering rate $1/\tau(\omega)$ and the optical mass enhancement factor $\lambda(\omega)$ are given by the following equations:

$$\frac{1}{\tau(\omega)} = \frac{n e^2}{m} \operatorname{Re} \left(\frac{1}{\sigma(\omega)} \right), \quad (2)$$

$$-\omega[1 + \lambda(\omega)] = \frac{n e^2}{m} \operatorname{Im} \left(\frac{1}{\sigma(\omega)} \right). \quad (3)$$

The contribution of all interband transitions has been subtracted from the obtained optical conductivity to take into account only the free-charge-carrier response. Lorentzian oscillators have been used to model the interband transitions by fitting the real and imaginary parts of the optical conductivity. The value of Ω_p^2 is calculated for each temperature and pressure by using

$$\Omega_p^2 = \frac{120}{\pi} \int_0^{\omega_c} \sigma_1(\omega) d\omega, \quad (4)$$

with the cutoff frequency ω_c taken as 2000 cm^{-1} .

The temperature-dependent optical scattering rate as calculated according to Eq. (2) is given in Fig. 3 for three pressures, namely, 1.3, 3, and 4.6 GPa in the frequency range up to 600 cm^{-1} . At 1.3 GPa [Fig. 3(a)] one observes a decrease of

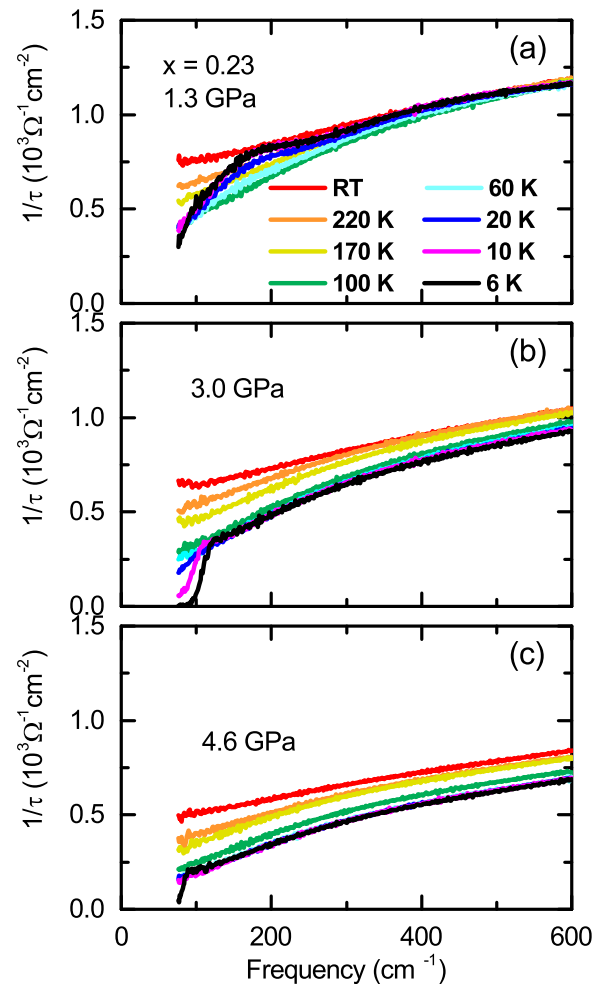


FIG. 3. Temperature-dependent optical scattering rate of BaFe₂(As_{0.77}P_{0.23})₂ at (a) 1.3, (b) 3.0, and (c) 4.6 GPa.

$1/\tau(\omega)$ in the $\omega \rightarrow 0$ limit with decreasing temperature, as expected for a metallic response, where one finds the narrowing of the Drude component with decreasing temperature. Below 60 K, $1/\tau(\omega)$ between 100 and 600 cm^{-1} starts to become higher than at 100 K, and with decreasing temperature a peaklike structure starts to grow which is a signature of the SDW order in the system [42]. At 6 K the signature of the SDW gap opening persists, and in addition a steep drop below 100 cm^{-1} indicates the existence of the SC state. A full SC transition is not visible due to the low-frequency-/temperature limit.

At 3.0 GPa [Fig. 3(b)] the signature of the SDW state in $1/\tau(\omega)$ is completely suppressed, and one observes an overall decrease of $1/\tau(\omega)$ with decreasing temperature down to T_c . Below 20 K a low-energy drop of $1/\tau(\omega)$ starts to develop, and with decreasing temperature a clear suppression of the scattering rate occurs below a certain energy due to the SC gap opening. The value of this energy slightly increases with decreasing temperature, indicating the increase of the SC gap. At 6 K a complete suppression of $1/\tau(\omega)$ below $\sim 90 \text{ cm}^{-1}$ is found. A further pressure increase does not change the principal behavior of $1/\tau(\omega)$. However, the suppression of the scattering rate due to the superconducting transition is much weaker compared to that at 3.0 GPa and is shifted to the lower-energy range, as illustrated by the temperature-dependent $1/\tau(\omega)$ spectra at 4.6 GPa [Fig. 3(c)].

With increasing pressure the overall optical scattering rate decreases in the given energy range, indicating the increase of the metallicity. A closer look shows that the decrease of $1/\tau(\omega)$ is persistent for all the temperatures (except the SDW range, where peaklike structures have been observed). Moreover, the almost temperature independent high-energy part starts to become more temperature dependent for higher pressures. This behavior is consistent with a change toward a Fermi-liquid state, which predicts a quadratic frequency dependence as the correspondent of the quadratic temperature dependence of the scattering rate. Even though the increase of the metallic behavior is clear, one should note that the system does not go into the Fermi-liquid state since an ω^2 behavior of $1/\tau(\omega)$ is not visible.

C. Electron-boson spectral density function

The pressure effects on the superconductivity in iron pnictide superconductors are very striking. Despite the lack of any chemical dopant, we actually can observe superconductivity with indications similar to those for the doped cases. This poses the question of what the mechanism of superconductivity induced by pressure in these materials could be. Evaluating the electron-boson spectral density $\alpha^2 F(\omega)$ under pressure may help to compare the effects of external pressure with those of doping.

The function $\alpha^2 F(\omega)$ describes an effective electron-electron interaction due to any kind of boson exchange mechanism. Hints of these bosonic excitations have been observed by many experimental methods such as ARPES [19], with which one can see the momentum-resolved bosonic contributions to the self-energy of the quasiparticles; STS [43], with which the contribution of the bosonic excitations with a spatial resolution of a unit cell can be detected; and infrared

spectroscopy [22], which can be used on a larger variety of materials and can be combined with other techniques like external pressure.

Detailed studies have been done with an infrared spectroscopy technique on another class of high-temperature superconductors, namely, cuprates [22,25,44]. Doping- and temperature-dependent boson functions have been obtained, and the differences compared to conventional superconductors have been put forward. When the Fe-Pn compounds as a new class of high- T_c superconductors were discovered, several similarities with the cuprates were observed, and hence, attempts to obtain the boson density function in a similar manner have been made [30–32,45]. One should note that Fe-Pn superconductors are multiband systems as opposed to the cuprates. Involving the multiband model in the numerical calculations will make the calculations much more complicated and beyond our capability to produce in this work. Therefore, in this work, we also implemented the previously applied numerical techniques based on the single-band assumption. Even though this may not be completely ideal, we can give the main implications, and it will be possible to compare the obtained results with the doped cases.

One can obtain $\alpha^2 F(\omega)$ from the optical scattering rate via the inversion of the following equation [46]:

$$\frac{1}{\tau(\omega, T)} = \frac{1}{\tau_{imp}} + \int_0^\infty [K(\omega, \Omega, T) \alpha^2 F(\omega)] d\Omega. \quad (5)$$

Here, $1/\tau_{imp}$ is the optical impurity scattering. $K(\omega, \Omega, T)$ is the kernel in the normal state at finite temperature [47]:

$$K(\omega, \Omega, T) = \frac{\pi}{\omega} \left[2\omega \coth\left(\frac{\Omega}{2T}\right) - (\omega + \Omega) \coth\left(\frac{\omega + \Omega}{2T}\right) + (\omega - \Omega) \coth\left(\frac{\omega - \Omega}{2T}\right) \right]. \quad (6)$$

For the superconducting state another kernel has been used [44]:

$$K(\omega, \Omega, T = 0) = \frac{2\pi}{\omega} (\omega - \Omega) \theta(\omega - 2\Delta_0 - \Omega) \times E\left(\sqrt{1 - \frac{4\Delta_0^2}{(\omega - \Omega)^2}}\right). \quad (7)$$

In this kernel the superconducting gap is assumed to be an isotropic s -wave gap in the clean limit. $E(x)$ is the complete elliptical integral of the second kind, $\theta(x)$ is the Heaviside function, with $\theta(x < 0) = 0$ and $\theta(x > 0) = 1$, and Δ_0 is the isotropic gap.

Several methods have been used in the literature to obtain the electron-boson spectral function $\alpha^2 F(\omega)$, such as the so-called second-derivative method, least-squares fitting (LSF), single-value determination (SVD), and the maximum entropy method (MEM). The limitations and advantages of these methods have been discussed previously [44]. One of the commonly seen problems in some of these techniques is the negative tails of the obtained boson function, which are unphysical and come solely from the numerical constraints. Even though earlier studies [48] tried to interpret them, later, they were mostly ignored. In the MEM method, the process of obtaining $\alpha^2 F(\omega)$ has been generalized to give strictly

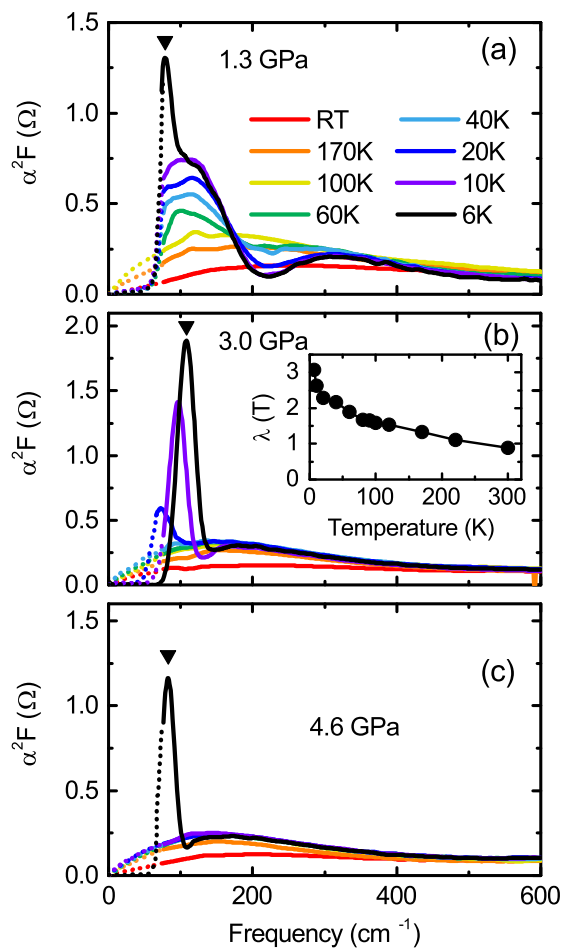


FIG. 4. Temperature-dependent boson spectral function $\alpha^2 F(\Omega)$ of BaFe₂(As_{0.77}P_{0.23})₂ at (a) 1.3, (b) 3.0, and (c) 4.6 GPa. Solid triangles mark the energy position of the sharp resonance peak associated with superconductivity. Inset: Temperature dependence of the electron-boson coupling constant λ at 3 GPa.

positive results. Moreover, in this method one does not need background information about the boson function, while in some other methods, like the LSF method, one should give an initial guess. Here, we also employed the MEM method for the deconvolution of Eq. (5). The resulting boson spectral function as a function of energy, temperature, and pressure is shown in Fig. 4 for three selected pressures.

In the normal state, a broad spectral weight distribution with a broad maximum at $\sim 250 \text{ cm}^{-1}$ at room temperature is apparent for all pressures. With decreasing temperature the broad maximum shifts to lower energies concurrent with a spectral weight increase. Note that the dotted part of the data in the low-energy region is, in principle, out of the measurement and observation range and therefore is extrapolated using a method similar to that used for the imaginary part of the complex dynamical spin susceptibility [49,50] due to the similarities of the spectral shapes. However, no discussion involving this energy range will be given since the extrapolation is only an approximation and the real behavior cannot be known. These extrapolations are just additions to the low-energy region via the calculated functions and hence do not affect the results in the measured energy range.

At 1.3 GPa [see Fig. 4(a)], a very dominant peaklike structure starts to appear below 60 K, which becomes more pronounced with decreasing temperature as an indication of the SDW state. At 6 K, a sharp resonance peak in addition to the peaklike structure develops, which is associated with the superconducting transition. At 3 GPa [Fig. 4(b)], the peaklike structure associated with the SDW state is no longer visible, and below 20 K a very clear resonance peak can be observed, indicating the SC gap opening. With a further temperature decrease the resonance peak shifts to higher energies and grows in intensity. For a pressure of 4.6 GPa [Fig. 4(c)] a behavior of $\alpha^2 F(\omega)$ like that at 3 GPa is observed. A broad background in the normal state that shifts to the lower-energy range with decreasing temperature evolves into a resonance peak below T_c .

The pressure and temperature dependences of the observed sharp resonance peak associated with the superconductivity show several interesting points. First, the resonance peak initially shifts to higher energies with increasing pressure up to a pressure of 3 GPa and then shifts back to lower energies with a further pressure increase (see solid triangles in Fig. 4). A detailed analysis of the pressure dependence reveals that the energy position of the resonance peak (energy of the peak maximum) follows the SC dome at 6 K. As an example, we plotted in Fig. 5(a) its energy position as a function of pressure at 6 K. Second, the temperature dependence of the energy of this resonance mode for a given pressure follows approximately an order-parameter-like evolution, i.e., $\Omega_R = \Omega_0 \sqrt{(1 - T/T_c)}$, as demonstrated in Fig. 5(b) for a pressure of 3.0 GPa. However, since extensive data for the temperature dependence are lacking, a detailed discussion cannot be given on this point. Also shown in Fig. 5(b) is a corresponding fit, and the so-obtained fitting parameters are $\Omega_0 = 118 \text{ cm}^{-1}$ and $T_c = 32 \text{ K}$. This transition temperature is consistent with the results from magnetic susceptibility measurements for this compound at the same pressure [11].

The energy of the observed resonance mode follows the SC dome, and its temperature dependence shows an order-parameter-like behavior. Both findings give strong evidence for the opening of the superconducting gap. However, the resonance mode does not necessarily indicate the magnetic pairing mechanism by itself. Sufficient spectral weight of the obtained boson function above T_c is a prerequisite of the boson pairing. Therefore, an examination of the normal-state spectral function and its redistribution below T_c is important.

One can check whether the spectral weight of $\alpha^2 F(\Omega)$ already present above T_c is enough to account for the superconductivity by estimating the maximum T_c^{max} using the generalized McMillan equation [51]:

$$k_B T_c^{max} \approx 1.13 \hbar \omega_{ln} \exp[-(\lambda + 1)/\lambda]. \quad (8)$$

Here, λ is the coupling constant, and ω_{ln} is the logarithmically averaged frequency, which can be calculated by

$$\lambda \equiv 2 \int_0^{w_c} \frac{\alpha^2 F(\Omega)}{\Omega} d\Omega, \quad (9)$$

$$\omega_{ln} \equiv \exp \left[\frac{2}{\lambda} \int_0^{w_c} \ln \Omega \frac{\alpha^2 F(\Omega)}{\Omega} d\Omega \right], \quad (10)$$

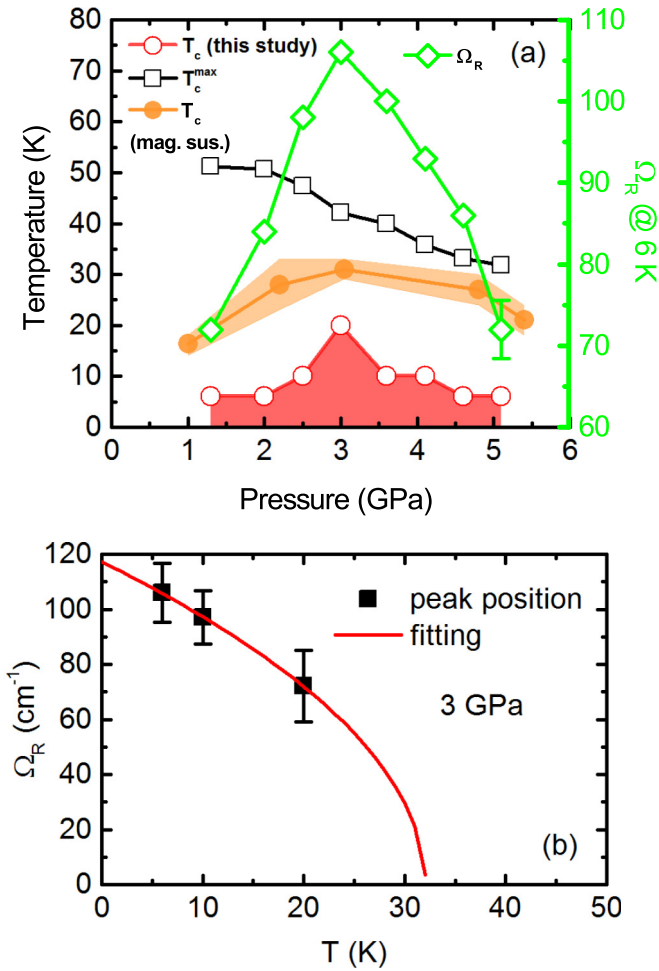


FIG. 5. Superconducting state in $\text{BaFe}_2(\text{As}_{0.77}\text{P}_{0.23})_2$: (a) Pressure dependence of the sharp resonance peak in $\alpha^2 F(\Omega)$ at 6 K (diamonds), along with the superconducting dome obtained from this measurement (open circles), magnetic susceptibility measurements (solid circles) [11], and pressure dependence of the estimated maximum T_c obtained with McMillan's formula (open squares). (b) Temperature dependence of the energy of the $\alpha^2 F(\Omega)$ resonance peak in the superconducting state at 3.0 GPa.

where ω_c is the cutoff frequency and has been set to 800 cm^{-1} . The temperature dependence of the coupling constant λ at 3.0 GPa is given in the inset of Fig. 4(b).

The values of T_c^{max} that can be obtained from the spectral weight of $\alpha^2 F(\Omega)$ in the normal state were calculated according to Eq. (8) for all pressures, and the results are plotted in Fig. 5(a) (squares) together with the T_c values obtained in the magnetic susceptibility measurements [11] (solid circles). Since T_c^{max} is larger than T_c for a given pressure, the observed spectral weight of the boson pairing in the normal state is sufficient to support the superconductivity with the observed T_c values in the whole studied pressure range. It is interesting to note that the T_c^{max} values do not follow a dome-like behavior, unlike the measured T_c values, and there is a distinctly different behavior in the low-pressure regime which also corresponds to the coexistence region of the SDW and SC states. This suggests that the system, in principle, can sustain a superconducting state up to ~ 50 K, but probably, the existence of the SDW state

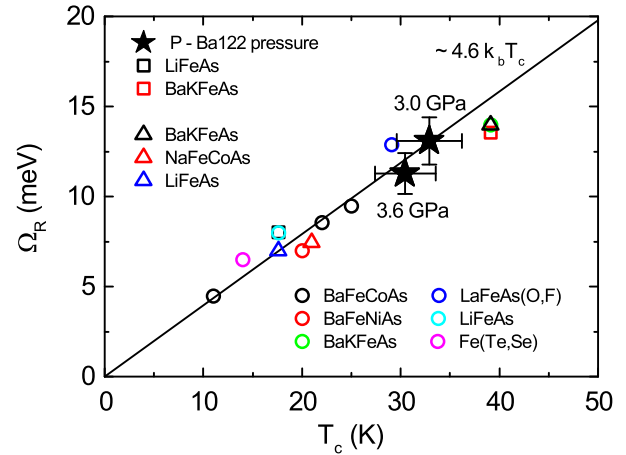


FIG. 6. Universal relation between T_c and the resonance frequency of the bosonic mode. Stars are the data obtained in this study from the resonance peak of $\alpha^2 F(\Omega)$. Open squares are the corresponding data from other ambient-pressure infrared studies [45], open triangles are obtained from STS measurements [43], and open circles correspond to the resonance peak of INS measurements [52].

prevents such a high SC transition temperature, indicating that the SDW might be a competing order to superconductivity.

Generally, one cannot distinguish the source of these bosonic excitations that seem to give rise to the superconductivity in the material. Some conclusions, however, can be drawn based on the comparison with other experimental methods such as INS, with which one can see the spin channel. Furthermore, band structure calculations can give some idea about the coupling constant of the phononic contributions. A detailed temperature-dependent INS study has been performed on $\text{BaFe}_{81.85}\text{Co}_{0.15}\text{As}_2$ ($T_c \sim 25$ K) [52], which is an optimally doped sample. According to our results, the optimum pressure with the maximum superconducting gap is observed at 3.0 GPa within our pressure resolution. Therefore, it is interesting to compare the properties observed for this pressure with the other optimally doped cases, where, indeed, the obtained electron-boson spectral function at 3.0 GPa shows several similarities. For instance, both the INS results and $\alpha^2 F(\Omega)$ obtained in this study show a similar broad background at room temperature, where the maximum shifts to lower energies with decreasing temperature. A resonance peak appears below T_c , where the energy of this mode shifts to higher energies with decreasing temperature and follows a superconducting order-parameter-like behavior. The resonance peak observed in our study is located at slightly higher energies compared to $\text{BaFe}_{81.85}\text{Co}_{0.15}\text{As}_2$, which can be explained by the higher transition temperature of $\text{BaFe}_2(\text{As}_{0.77}\text{P}_{0.23})_2$ under pressure.

The coupling to a bosonic mode in iron pnictide superconductors has been observed with several experimental methods, such as infrared spectroscopy [30,31], INS [52], and STS [43]. These observations are not unique to the so-called 122 iron pnictide family either. Other classes of iron pnictides, such as LiFeAs , also showed similar coupling behavior [45,53]. It has been shown that the mode energy versus T_c follows a universal curve for the iron pnictides, where the slope is given by $\Omega_R \sim 4.6 k_b T_c$. We present this universal curve in Fig. 6 based on

the results of various experimental methods, namely, infrared spectroscopy [45] (open squares), STS [43] (open triangles), and INS [52] (open circles). We also included the resonance energies obtained from this study (solid stars) for 3.0 and 3.6 GPa, where a full SC transition has been observed. As one can see, the results obtained in our study match the universal curve very well. Several similarities observed between the pressure- and doping-induced superconductivities in the spin-channel suggest that the pressure-induced superconductivity in P-Ba122 could be spin fluctuation mediated.

The calculated T_c^{max} as a function of pressure has already been discussed and is given in Fig. 5(a) (squares), and it was shown that it can support the observed T_c values. One notices that in the normal state the spectral weight of the electron-boson function decreases with increasing pressure, which results in the decrease of the estimated T_c^{max} . This finding may indicate the weakening of the spin fluctuations with increasing pressure, which is consistent with the suppression of the SDW under pressure (see Fig. 2).

It is interesting to note that the energy range of the resonance peak is also compatible with the alternative scenario of phonon-mediated superconductivity. However, the electron-phonon coupling strength calculated for Fe-Pn significantly deviates from the values obtained in this study. The temperature-dependent coupling constant is depicted in the inset of Fig. 4(b). Coupling constants $\lambda \sim 0.21$ for the 1111 family [54] of Fe-Pn and $\lambda < 0.2$ for EuFe₂As₂, BaFe₂As₂, SrFe₂As₂, and BaFe_{1.85}Co_{0.15}As₂ ($T_c = 23$ K) have been reported [55,56], obtained using band structure calculations, Raman scattering, and time-resolved ARPES measurements. Obviously these values are much smaller than the value of $\lambda = 3.2$ for the present compound [see inset of Fig. 4(b)]. Such a high bosonic coupling constant obtained via infrared spectroscopy was reported previously for the 122 family of Fe-Pn systems as well [31]. Therefore, even though the energy range is reasonable, a phonon-mediated mechanism for superconductivity seems to be unlikely for the investigated system. Note that the contributions of the phonons cannot be completely ruled out. However, much stronger contributions seem to dominate the obtained boson function, and taking into account the similarities with the INS measurements, we conclude that these contributions might be spin fluctuations.

We also remark on the low-energy pseudogap that has previously been reported for the iron pnictides from infrared spectroscopy studies via electron-boson spectral analysis [57,58]. In these studies, the opening of a pseudogap state at the Fermi energy of the density of states has been traced with the boson spectral density, and the emergence of a peaklike structure associated with the pseudogap opening above T_c has been observed. Besides the pseudogap opening, low-energy interband transitions might give a similar contribution to the boson function [59]. In our study no additional structure has been observed besides the peaklike structures appearing below T_c and T_N (at low pressures). In the low-pressure regime, the spectra above T_c , where one might expect a pseudogap (or low-energy interband transitions), is mainly dominated by the SDW state. This might be the reason why we cannot resolve the pseudogap behavior, which other studies reported for the optimally doped samples without a SDW ordered state. For higher pressures, where no SDW state exists, a structure of the

electron-boson spectral density associated with a pseudogap still could not be observed, either because the effect is too small to resolve or because it is suppressed by external pressure.

D. Superconducting gap

We observed a complete transition to the superconducting state with the largest energy gap at the 3.0-GPa pressure (optimum pressure). In Fig. 7 the measured reflectivity and the calculated optical conductivity, obtained by the KK transformation of the measured reflectivity, are given for this optimum pressure. The increasing reflectivity with decreasing temperature and decreasing frequency indicates the metallic behavior of the system. The steplike behavior in the reflectivity spectrum below ~ 200 cm⁻¹ at 6 K shows a clear superconducting transition. Correspondingly, at 6 K the gradual suppression of the optical conductivity is found in the low-energy region [see Fig. 7(b)], which eventually is fully suppressed below ~ 90 cm⁻¹. This full suppression indicates the nodeless nature of the superconducting gap under pressure.

To extract the superconducting gap value, the optical conductivity spectrum in the SC region has been analyzed using the Mattis-Bardeen approximation [60,61]. Two isotropic gaps with estimated gap values $\Delta_{SC,1} \approx 6.0$ meV and

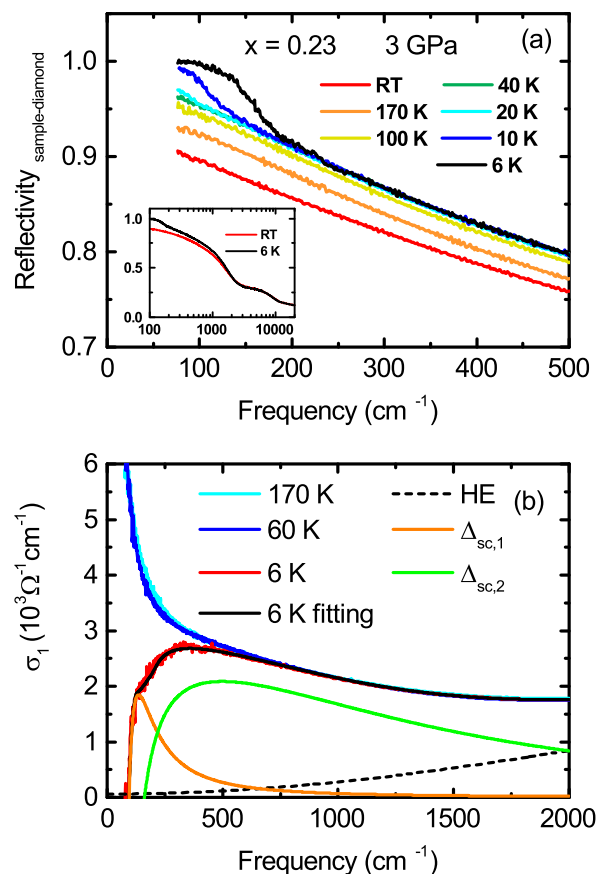


FIG. 7. (a) Temperature-dependent reflectivity spectra of BaFe₂(As_{0.77}P_{0.23})₂ at 3.0 GPa. Inset: Reflectivity spectra at RT and 6 K up to higher energies. (b) Components of the optical conductivity in the superconducting state (at 6 K): small ($\Delta_{SC,1}$) and large ($\Delta_{SC,2}$) gap components and high-energy contributions (HE).

$\Delta_{SC,2} \approx 10.4$ meV can reproduce our optical conductivity spectrum. These values are very similar to the ones for other iron pnictide systems [62] with similar T_c , as well as for the parent compound BaFe_2As_2 under pressure [34].

In previous studies, the P-doped Ba122 system was suggested to show a nodal gap structure [63], in contrast to what we observed in this study. One possible explanation is that a crossover from nodal to nodeless superconductivity is induced under external pressure in this system. Similar crossover behavior has been widely observed for the systems where one dopes P to As sites, such as LiFeAs (nodeless SC)/ LiFeP (nodal SC) and LaFeAsO (non-SC)/ LaFePO (nodal SC). Therefore, general unified relations between structural parameters of iron pnictides (pnictogen height h_{pn} , bond angle α , Fe-Fe atom distance, etc.) and nodeless/nodal SC have been proposed [64–66].

One of these proposals is also plausible for our case, namely, h_{pn} being the switch between nodal and nodeless superconductivities [65]. Reference [65] proposed that the pnictogen height h_{pn} can be used as the tuning parameter, where one can see a crossover from low- T_c nodal SC to high- T_c nodeless SC with increasing h_{pn} . There are no x-ray diffraction data under pressure available for the P-doped Ba122 system, from which the lattice and other structural parameters could be obtained for $\text{BaFe}_2(\text{As}_{0.77}\text{P}_{0.23})_2$ under pressure. However, such studies have been performed on the Ba122 parent compound [10,67]: it has been shown that the bond angle α decreases with increasing pressure, while the pnictogen height h_{pn} shows an opposite effect, namely, an increase with increasing pressure. We also expect a qualitatively similar effect of pressure on the structural parameters of P-doped Ba122, even though a quantitative discussion cannot be given. If this is indeed the case for P-doped Ba122, then the change in the gap structure under pressure could be linked to the Fermi-surface reconstruction, which is triggered by the structural changes [65]. One should keep in mind that the theory has been generalized for the 1111 Fe-Pn system $\text{LaFeAsO}/\text{LaFeAsP}$. The change in the Fermi-surface topology with a change in the structural parameters can be significantly different in the case of P-doped Ba122 under pressure. To give a more solid discussion of the nodal/nodeless SC issue this study alone is not enough.

Another possible explanation for the observed nodeless SC state under pressure is that perhaps infrared spectroscopy is not sensitive enough to trace the nodes with $E \parallel ab$ -plane measurements, while other measurement techniques such as specific-heat measurements can detect these nodes. It is worth pointing out that other infrared spectroscopy measurements of the P-doped Ba122 system at ambient pressure, where a much lower-energy region can be reached compared to that in our study, did not report the existence of the nodes either [57].

E. Electronic correlations

Finally, we will focus on the pressure dependence of the electronic correlations in the P-doped Ba122 compound. We followed the procedure given in previous studies for Fe-Pn compounds [68] as described below, and the results are presented in Fig. 8.

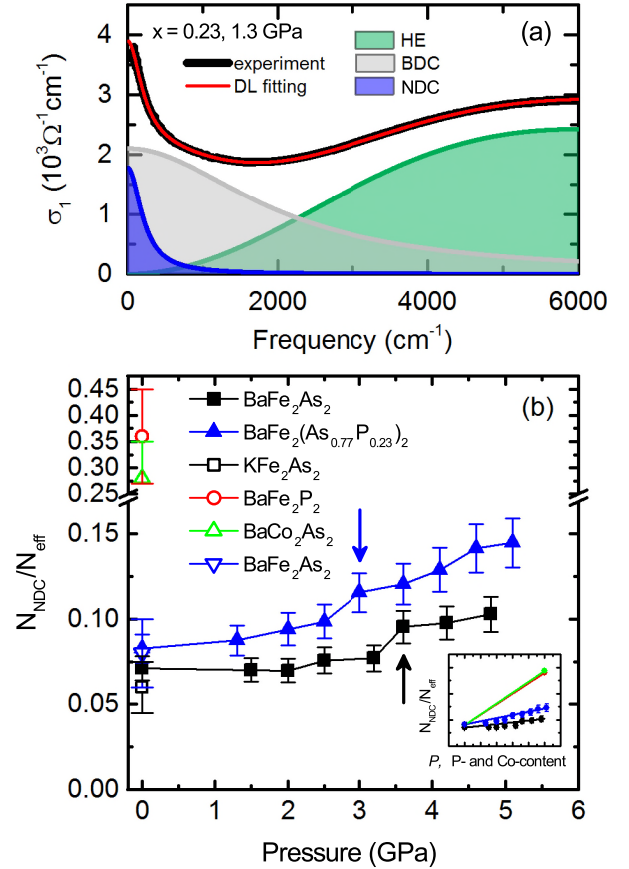


FIG. 8. (a) Room-temperature optical conductivity of $\text{BaFe}_2(\text{As}_{0.77}\text{P}_{0.23})_2$ at 1.3 GPa with the Drude-Lorentz (DL) fitting and the contributions [high-energy (HE), broad Drude component (BDC), and narrow Drude component (NDC)]. (b) Pressure dependence of the electronic correlation strength. Open symbols are given for comparison at ambient pressure [69]. Arrows indicate the optimum pressure ranges for the given compounds. Inset: Electronic correlation strength with pressure [for $\text{BaFe}_2(\text{As}_{1-x}\text{P}_x)_2$ with $x = 0$ and 0.23] and P and Co doping. P and Co contents have been normalized to pressure based on the change in the c -axis lattice constant [67,70,71].

The optical conductivity spectra can be described by two Drude components [narrow Drude component (NDC) and broad Drude component (BDC)] in the lower-energy region, indicating the multiband character of the Fe-Pn compounds, and one Lorentzian contribution in the higher-energy range corresponding to interband excitations [see Fig. 8(a)] [35,69,72]. The spectral weight of the NDC and BDC components can be calculated according to

$$N_{NDC,BDC}(\omega) = \int_0^{\omega_c} \sigma_1(\omega) d\omega. \quad (11)$$

The Drude contributions were extracted from the total optical conductivity by Drude-Lorentz model fitting, and the integration was carried out with a cutoff frequency $\omega_c \sim 10000$ cm^{-1} . The covered energy range is high enough to encounter all the spectral weight of the components, and above this energy range the tail of the Drude components is negligible.

The fraction of the narrow Drude weight N_{NDC}/N_{eff} , where N_{eff} is the effective carrier number and can be calculated as $N_{eff} = N_{NDC} + N_{BDC}$, is a measure of the degree of coherence of the carrier dynamics and was suggested as a measure of electronic correlations [68]. In Fig. 8(b) the pressure dependence of the electronic correlations is plotted for the parent compound ($x = 0$) and the P-doped sample ($x = 0.23$). In the case of the P-doped sample the ratio N_{NDC}/N_{eff} at ambient pressure is slightly higher than that of the parent compound; that is, P doping slightly decreases the correlations. Moreover, a small decrease of the electronic correlations with increasing pressure is found in both cases. A closer look at the pressure dependence reveals that the decrease of the correlations is actually discontinuous, and it shows a small jump at 3.6 GPa for $x = 0$ [34] and at 3.0 GPa for $x = 0.23$, indicated by arrows in Fig. 8(b). Note that these pressures are the optimum pressures with the maximum superconducting gap.

Importantly, external pressure seems to be not as effective as isovalent and electron doping (compared to the other end materials) regarding the influence on electronic correlations since in the isovalent and electron doping cases a much stronger decrease of the electronic correlations has been observed [69]. A comparison is given in the inset of Fig. 8(b), where the P and Co contents have been normalized to pressure based on the change in the c -axis lattice constant [67,70,71]. Under pressure, the correlation range remains small and shows a behavior similar to that of the hole-doped case (for example KFe₂As₂). The similarities of hole doping and external pressure on other parameters like pnictogen height and bond angle have also been shown previously [34]. This may indicate that external pressure mainly affects the hole Fermi surfaces rather than electron ones. Indeed, hole doping with external pressure has been suggested by band calculations for the 1111 Fe-Pn systems [73]; however, such calculations are lacking for the 122 Fe-Pn.

F. Phase diagram

The results of our present optical studies, together with the results from previous optical, electrical transport, and magnetic susceptibility measurements [3,8,9,11,34,69], are summarized in the phase diagram of BaFe₂(As_{1-x}P_x)₂ as a function of pressure, temperature, and P content presented in Fig. 9(a). The main trends illustrated in the phase diagram are the following: The SDW state is suppressed with increasing pressure and increasing P content x . For $x = 0$, in the whole measured pressure range an SDW state was observed, even though T_N is reduced from 138 to ~ 70 K under pressure. At 3.6 and 4.2 GPa an SC state coexisting with the SDW state has been observed for the parent compound using infrared spectroscopy [34]. Owing to the low-energy limit of the measurements, a full superconducting dome could not be observed; however, these two pressures are consistent with the highest observed T_c in transport measurements [3,8,9]. The coexistence region for the parent compound (from electrical transport measurements) extends up to ~ 9 GPa.

The compound with $x = 0.23$ is superconducting at ambient pressure with $T_N \sim 70$ K. Due to the lack of electrical transport measurements under pressure, the behavior of the

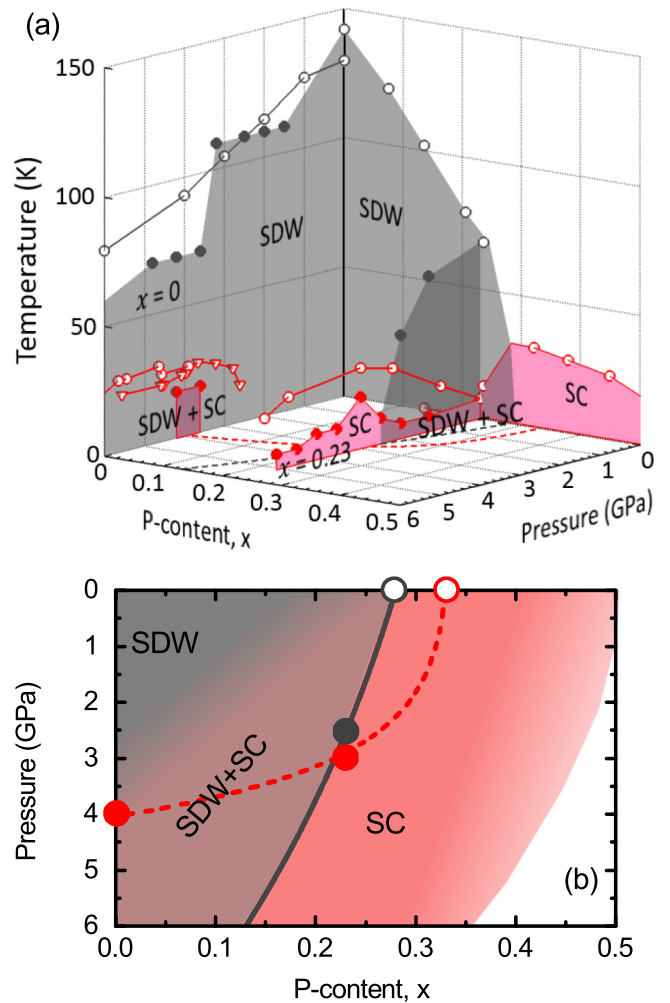


FIG. 9. Solid symbols are from this study, while open symbols are from electrical transport and magnetic susceptibility measurements [3,8,9,11,69]. (a) Pressure-, temperature-, and P-content-dependent phase diagram of BaFe₂(As_{1-x}P_x)₂. (b) The SDW, SC, and coexistence region as a function of pressure and P content at 6 K. Gray circles trace the coexistence-region to SC-state crossover, while red circles show the optimum pressures at each P content. The gray solid and red dashed lines are guides to the eye. Note that the gray curve is extended to the higher-pressure range for the parent compound.

SDW state was unknown. However, in the current infrared spectroscopy study we traced the suppression of the SDW state with increasing pressure, and the disappearance of this state at ~ 2.5 GPa was observed. Moreover, the overall SC dome could also be traced and is consistent with earlier magnetic susceptibility measurements [11].

In Fig. 9(b), we plot the SDW, SC, and coexistence region as a function of pressure and P content at 6 K. Gray circles trace the pressure range where the SDW state is suppressed completely and hence the coexistence region is terminated. The solid gray curve is given as a guide to the eye; moreover, it combines the shown points with the parent compound in the higher-pressure range. For the parent compound, this point is determined from the electrical resistivity measurements [3,74], while infrared spectroscopy was not conclusive enough

(the pressure reached was not high enough to suppress the SDW state completely). As one can see, this suppression occurs in a nonlinear fashion with increasing P content. The red circles mark the pressure values at which the maximum T_c (optimum pressure) has been observed for each sample. The red dashed line is a guide to the eye that traces the optimum pressure with increasing P content, where infrared spectroscopy, electrical transport, and magnetic susceptibility measurements are consistent. Similar to the SDW state, the decrease of the optimum pressure with P content is rather sharp and follows a steep nonlinear behavior. With high enough pressure a SC dome could also be observed [11]. On the other hand, on reaching the optimum doping ($x \sim 0.33$ for $\text{BaFe}_2(\text{As}_{1-x}\text{P}_x)_2$ [68]), pressure suppresses the superconductivity.

IV. CONCLUSIONS

Temperature- and pressure-dependent reflectivity measurements have been carried out on $\text{BaFe}_2(\text{As}_{0.77}\text{P}_{0.23})_2$ single crystals, and the results have been compared to those for the parent compound BaFe_2As_2 . The pressure-induced superconducting state in $\text{BaFe}_2(\text{As}_{0.77}\text{P}_{0.23})_2$ has been investigated in terms of the electron-boson spectral function. The results showed the appearance of a sharp resonance mode below T_c , with a superconducting domelike energy dependence. Moreover, the temperature dependence of the resonance mode follows a superconducting order-parameter-like behavior demonstrating the relation of the resonance mode to the superconducting gap opening.

The obtained electron-boson spectral function also shows several similarities to the boson mode that is discussed in STS and INS dynamical spin susceptibility in the literature, suggesting a possible spin-fluctuation mechanism for the

superconductivity under pressure. Moreover, the energy range of the resonance mode follows a $\Omega_R/k_b T_c \sim 4.6$ universal curve.

Pressure effects on the parent compound Ba122 and P-doped Ba122 samples have also been compared. The evolution of the electronic correlations and the phase diagram show similar behavior for both compounds. The suppression of the SDW state and the emergence of the SC state with increasing pressure have been observed. Moreover, the coexistence of the SDW and SC state has been shown in both cases. Also the obtained maximum T_c and the superconducting gaps are similar in the optimum pressure range. With increasing P content, the pressure ranges where one can observe the SDW state and the highest SC transition temperature shift to the lower-pressure regime in a nonlinear fashion. Such behavior is expected since the P-doped compound possesses weaker SDW order and is already superconducting at ambient pressure, and hence, the suppression of the SDW state and the increase of the superconductivity are observed faster with increasing pressure.

ACKNOWLEDGMENTS

We thank M. Nakajima for the UV-region reflectivity data, D. Schmitz and W. Scherer for the magnetic susceptibility measurements, and E. Üretürk Yetişmiş for discussions during the data analysis. We also would like to acknowledge fruitful discussions with R. Valentí, H. Jeschke, and M. Tomić. E.U. acknowledges financial support from the Bavarian Research Foundation. C.A.K. and E.U. acknowledge financial support from the Federal Ministry of Education and Research (BMBF), Germany, through Grant No. 05K13WA1 (Verbundprojekt 05K2013, Teilprojekt 1, PT-DESY). The work in Japan is supported by IRON-SEA, Japan Science and Technology Agency (JST).

-
- [1] M. S. Torikachvili, S. L. Bud'ko, N. Ni, and P. C. Canfield, *Phys. Rev. Lett.* **101**, 057006 (2008).
 - [2] M. S. Torikachvili, S. L. Bud'ko, N. Ni, and P. C. Canfield, *Phys. Rev. B* **78**, 104527 (2008).
 - [3] P. L. Alireza, Y. T. C. Ko, J. Gillett, C. M. Petrone, J. M. Cole, G. G. Lonzarich, and S. E. Sebastian, *J. Phys. Condens. Matter* **21**, 012208 (2009).
 - [4] H. Kotegawa, T. Kawazoe, H. Sugawara, K. Murata, and H. Tou, *J. Phys. Soc. Jpn.* **78**, 083702 (2009).
 - [5] F. Ishikawa, N. Eguchi, M. Kodama, K. Fujimaki, M. Einaga, A. Ohmura, A. Nakayama, A. Mitsuda, and Y. Yamada, *Phys. Rev. B* **79**, 172506 (2009).
 - [6] K. Igawa, H. Okada, H. Takahashi, S. Matsuishi, Y. Kamihara, M. Hirano, H. Hosono, K. Matsubayashi, and Y. Uwatoko, *J. Phys. Soc. Jpn.* **78**, 025001 (2009).
 - [7] N. Kurita, M. Kimata, K. Kodama, A. Harada, M. Tomita, H. S. Suzuki, T. Matsumoto, K. Murata, S. Uji, and T. Terashima, *Phys. Rev. B* **83**, 100501 (2011).
 - [8] E. Colombier, S. L. Bud'ko, N. Ni, and P. C. Canfield, *Phys. Rev. B* **79**, 224518 (2009).
 - [9] K. Ahilan, J. Balasubramaniam, F. L. Ning, A. S. Imai, T. Sefat, R. Jin, B. C. McGuire, M. A. Sales, and D. Mandrus, *J. Phys. Condens. Matter* **20**, 472201 (2008).
 - [10] S. Drotziger, P. Schweiss, K. Grube, T. Wolf, P. Adelman, C. Meingast, and H. v. Löhneysen, *J. Phys. Soc. Jpn.* **79**, 124705 (2010).
 - [11] L. E. Klintberg, G. S. K., S. Kasahara, Y. Nakai, K. Ishida, M. Sutherland, T. Shibauchi, Y. Matsuda, and T. Terashima, *J. Phys. Soc. Jpn.* **79**, 123706 (2010).
 - [12] J. P. Carbotte, *Rev. Mod. Phys.* **62**, 1027 (1990).
 - [13] V. J. Emery and S. Kivelson, *Nature (London)* **374**, 434 (1995).
 - [14] J. P. Carbotte, E. Schachinger, and D. Basov, *Nature (London)* **401**, 354 (1999).
 - [15] J. Lee, K. Fujita, K. McElroy, J. A. Slezak, M. Wang, Y. Aiura, H. Bando, M. Ishikado, T. Masui, J.-X. Zhu, A. V. Balatsky, H. Eisaki, S. Uchida, and J. C. Davis, *Nat. Lett.* **442**, 546 (2006).
 - [16] P. J. Hirschfeld, M. M. Korshunov, and I. I. Mazin, *Rep. Prog. Phys.* **74**, 124508 (2011).
 - [17] A. Chubukov, *Annu. Rev. Condens. Matter Phys.* **3**, 57 (2012).
 - [18] H. Hosono and K. Kuroki, *Phys. C (Amsterdam, Neth.)* **514**, 399 (2015).

- [19] A. Damascelli, Z. Hussain, and Z.-X. Shen, *Rev. Mod. Phys.* **75**, 473 (2003).
- [20] B. Muschler, W. Prestel, E. Schachinger, J. P. Carbotte, R. Hackl, S. Ono, and Y. Ando, *J. Phys. Condens. Matter* **22**, 375702 (2010).
- [21] T. Hanaguri, K. Kitagawa, K. Matsubayashi, Y. Mazaki, Y. Uwatoko, and H. Takagi, *Phys. Rev. B* **85**, 214505 (2012).
- [22] J. P. Carbotte, T. Timusk, and J. Hwang, *Rep. Prog. Phys.* **74**, 066501 (2011).
- [23] B. Farnworth and T. Timusk, *Phys. Rev. B* **10**, 2799 (1974).
- [24] E. Schachinger and J. P. Carbotte, *Phys. Rev. B* **62**, 9054 (2000).
- [25] S. V. Dordevic, C. C. Homes, J. J. Tu, T. Valla, M. Strongin, P. D. Johnson, G. D. Gu, and D. N. Basov, *Phys. Rev. B* **71**, 104529 (2005).
- [26] J. Hwang, J. Yang, T. Timusk, S. G. Sharapov, J. P. Carbotte, D. A. Bonn, R. Liang, and W. N. Hardy, *Phys. Rev. B* **73**, 014508 (2006).
- [27] J. Hwang, T. Timusk, E. Schachinger, and J. P. Carbotte, *Phys. Rev. B* **75**, 144508 (2007).
- [28] E. Schachinger, C. C. Homes, R. P. S. M. Lobo, and J. P. Carbotte, *Phys. Rev. B* **78**, 134522 (2008).
- [29] E. van Heumen, E. Muhlethaler, A. B. Kuzmenko, H. Eisaki, W. Meevasana, M. Greven, and D. van der Marel, *Phys. Rev. B* **79**, 184512 (2009).
- [30] J. Yang, D. Huvonen, U. Nagel, T. Room, N. Ni, P. C. Canfield, S. L. Budko, J. P. Carbotte, and T. Timusk, *Phys. Rev. Lett.* **102**, 187003 (2009).
- [31] D. Wu, N. Barisic, M. Dressel, G. H. Cao, Z. A. Xu, E. Schachinger, and J. P. Carbotte, *Phys. Rev. B* **82**, 144519 (2010).
- [32] J. Hwang, J. P. Carbotte, B. H. Min, Y. S. Kwon, and T. Timusk, *J. Phys. Condens. Matter* **27**, 055701 (2015).
- [33] A. Charnukha, O. V. Dolgov, A. A. Golubov, Y. Matiks, D. L. Sun, C. T. Lin, B. Keimer, and A. V. Boris, *Phys. Rev. B* **84**, 174511 (2011).
- [34] E. Uykur, T. Kobayashi, W. Hirata, S. Miyasaka, S. Tajima, and C. A. Kuntscher, *Phys. Rev. B* **92**, 245133 (2015).
- [35] M. Nakajima, S. Ishida, K. Kihou, Y. Tomioka, T. Ito, Y. Yoshida, C. H. Lee, H. Kito, A. Iyo, H. Eisaki, K. M. Kojima, and S. Uchida, *Phys. Rev. B* **81**, 104528 (2010).
- [36] M. Nakajima, T. Liang, S. Ishida, Y. Tomioka, K. Kihou, C. H. Lee, A. Iyo, H. Eisaki, T. Kakeshita, T. Ito, and S. Uchida, *Proc. Natl. Acad. Sci. USA* **108**, 12238 (2011).
- [37] R. Keller and W. B. Holzapfel, *Rev. Sci. Instrum.* **48**, 517 (1977).
- [38] H. K. Mao, J. Xu, and P. M. Bell, *J. Geophys. Res.* **91**, 4673 (1986).
- [39] C. A. Kuntscher, A. Huber, and M. Hücker, *Phys. Rev. B* **89**, 134510 (2014).
- [40] A. Pashkin, M. Dressel, and C. A. Kuntscher, *Phys. Rev. B* **74**, 165118 (2006).
- [41] D. N. Basov and T. Timusk, *Rev. Mod. Phys.* **77**, 721 (2005).
- [42] D. Wu, N. Barišić, N. Drichko, S. Kaiser, A. Faridian, M. Dressel, S. Jiang, Z. Ren, L. J. Li, G. H. Cao, Z. A. Xu, H. S. Jeevan, and P. Gegenwart, *Phys. Rev. B* **79**, 155103 (2009).
- [43] Z. Wang, H. Yang, D. Fang, B. Shen, Q. Wang, L. Shan, C. Zhang, P. Dai, and H. Wen, *Nat. Phys.* **9**, 42 (2012).
- [44] E. Schachinger, D. Neuber, and J. P. Carbotte, *Phys. Rev. B* **73**, 184507 (2006).
- [45] J. Hwang, *J. Phys. Condens. Matter* **28**, 125702 (2016).
- [46] P. Allen, *Phys. Rev. B* **3**, 305 (1971).
- [47] S. Shulga, O. Dolgov, and E. Maksimov, *Phys. C (Amsterdam, Neth.)* **178**, 266 (1991).
- [48] Ar. Abanov, A. V. Chubukov, and J. Schmalian, *Phys. Rev. B* **63**, 180510 (2001).
- [49] A. Heimes, R. Grein, and M. Eschrig, *Phys. Rev. Lett.* **106**, 047003 (2011).
- [50] A. Heimes, R. Grein, and M. Eschrig, *Phys. Rev. B* **86**, 064528 (2012).
- [51] W. L. McMillan, *Phys. Rev.* **167**, 331 (1968).
- [52] D. S. Inosov, J. Park, P. Bourges, D. Sun, Y. Sidis, A. Schneidewind, K. Hradil, D. Haug, C. Lin, B. Keimer, and V. Hinkov, *Nat. Lett.* **6**, 178 (2010).
- [53] S. Chi, S. Grothe, R. Liang, P. Dosanjh, W. N. Hardy, S. A. Burke, D. A. Bonn, and Y. Pennec, *Phys. Rev. Lett.* **109**, 087002 (2012).
- [54] L. Boeri, O. V. Dolgov, and A. A. Golubov, *Phys. Rev. Lett.* **101**, 026403 (2008).
- [55] K.-Y. Choi, P. Lemmens, I. Eremin, G. Zwirgagl, H. Berger, G. L. Sun, D. Sun, and C. Lin, *J. Phys. Condens. Matter* **22**, 115802 (2010).
- [56] L. Rettig, R. Cortés, H. Jeevan, P. Gegenwart, T. Wolf, J. Fink, and U. Bovensiepen, *New J. Phys.* **15**, 083023 (2013).
- [57] S. J. Moon, A. A. Schafgans, S. Kasahara, T. Shibauchi, T. Terashima, Y. Matsuda, M. A. Tanatar, R. Prozorov, A. Thaler, P. C. Canfield, A. S. Sefat, D. Mandrus, and D. N. Basov, *Phys. Rev. Lett.* **109**, 027006 (2012).
- [58] S. J. Moon, Y. S. Lee, A. A. Schafgans, A. V. Chubukov, S. Kasahara, T. Shibauchi, T. Terashima, Y. Matsuda, M. A. Tanatar, R. Prozorov, A. Thaler, P. C. Canfield, S. L. Bud'ko, A. S. Sefat, D. Mandrus, K. Segawa, Y. Ando, and D. N. Basov, *Phys. Rev. B* **90**, 014503 (2014).
- [59] P. Marsik, C. N. Wang, M. Rössle, M. Yazdi-Rizi, R. Schuster, K. W. Kim, A. Dubroka, D. Munzar, T. Wolf, X. H. Chen, and C. Bernhard, *Phys. Rev. B* **88**, 180508 (2013).
- [60] D. C. Mattis and J. Bardeen, *Phys. Rev.* **111**, 412 (1958).
- [61] W. Zimmermann, E. H. Brandt, M. Bauer, E. Seider, and L. Genzel, *Phys. C (Amsterdam, Neth.)* **183**, 99 (1991).
- [62] D. S. Inosov, J. T. Park, A. Charnukha, Y. Li, A. V. Boris, B. Keimer, and V. Hinkov, *Phys. Rev. B* **83**, 214520 (2011).
- [63] K. Hashimoto, M. Yamashita, S. Kasahara, Y. Senshu, N. Nakata, S. Tonegawa, K. Ikada, A. Serafin, A. Carrington, T. Terashima, H. Ikeda, T. Shibauchi, and Y. Matsuda, *Phys. Rev. B* **81**, 220501(R) (2010).
- [64] H. Kinouchi, H. Mukuda, Y. Kitaoka, P. M. Shirage, H. Fujihisa, Y. Gotoh, H. Eisaki, and A. Iyo, *Phys. Rev. B* **87**, 121101 (2013).
- [65] K. Kuroki, H. Usui, S. Onari, R. Arita, and H. Aoki, *Phys. Rev. B* **79**, 224511 (2009).
- [66] K. Hashimoto, S. Kasahara, R. Katsumata, Y. Mizukami, M. Yamashita, H. Ikeda, T. Terashima, A. Carrington, Y. Matsuda, and T. Shibauchi, *Phys. Rev. Lett.* **108**, 047003 (2012).
- [67] S. A. J. Kimber, A. Kreyssig, Y. Z. Zhang, H. O. Jeschke, R. Valenti, F. Yokaichiya, E. Colombier, J. Yan, T. C. Hansen, T. Chatterji, R. J. McQueeney, P. C. Canfield, A. I. Goldman, and D. N. Argyriou, *Nat. Mater.* **8**, 471 (2009).
- [68] M. Nakajima, S. Ishida, T. Tanaka, K. Kihou, Y. Tomioka, T. Saito, C. H. Lee, H. Fukazawa, Y. Kohori, T. Kakeshita, A. Iyo, T. Ito, H. Eisaki, and S. Uchida, *Sci. Rep.* **4**, 5873 (2014).

- [69] M. Nakajima, T. Tanaka, S. Ishida, K. Kihou, C. H. Lee, A. Iyo, T. Kakeshita, H. Eisaki, and S. Uchida, *Phys. Rev. B* **88**, 094501 (2013).
- [70] S. Kasahara, T. Shibauchi, K. Hashimoto, K. Ikada, S. Tonegawa, R. Okazaki, H. Shishido, H. Ikeda, H. Takeya, K. Hirata, T. Terashima, and Y. Matsuda, *Phys. Rev. B* **81**, 184519 (2010).
- [71] N. Ni, M. E. Tillman, J.-Q. Yan, A. Kracher, S. T. Hannahs, S. L. Bud'ko, and P. C. Canfield, *Phys. Rev. B* **78**, 214515 (2008).
- [72] N. Barišić, D. Wu, M. Dressel, L. J. Li, G. H. Cao, and Z. A. Xu, *Phys. Rev. B* **82**, 054518 (2010).
- [73] D. Freitas, G. Garbarino, R. Weht, A. Sow, X. Zhu, F. Han, P. Cheng, J. Ju, H. Wen, and M. Regueiro, *J. Phys. Condens. Matter* **26**, 155702 (2014).
- [74] H. Fukazawa, N. Takeshita, T. Yamazaki, K. Kendo, K. Hirayama, Y. Kohori, K. Miyazawa, H. Kito, H. Eisaki, and A. Iyo, *J. Phys. Soc. Jpn.* **77**, 105004 (2008).